

# Electrochemistry of Catechol Terminated Monolayers with Cu(II), Ni(II) and Fe(III) Cations: A Model for the Marine Adhesive Interface

Paula A. Brooksby,<sup>\*,†</sup> David R. Schiel,<sup>‡</sup> and Andrew D. Abell<sup>§</sup>

Department of Chemistry, University of Canterbury, Private Bag 4800, Christchurch, New Zealand, Biological Sciences, University of Canterbury, Private Bag 4800, Christchurch, New Zealand, and School of Chemistry and Physics, The University of Adelaide, Adelaide, South Australia, 5005, Australia

Received March 12, 2008. Revised Manuscript Received June 1, 2008

The redox electrochemistry of hydroquinone and Cu<sup>2+</sup>–, Ni<sup>2+</sup>–, and Fe<sup>3+</sup>–hydroquinone complexes immobilized at the SAM interface has been studied in aqueous solutions with pH 5 to 12 using cyclic voltammetry. Self-assembled monolayers were constructed with terminal hydroquinone residues designed to model marine adhesive proteins that use the DOPA (3,4-dihydroxyphenylalanine) moiety. Coordination of metal to the hydroquinone group results in a shift to the ligand oxidation potential, with the value for  $\Delta E_{p,a}$  dependent on the solution pH and identity of the metal. Cu<sup>2+</sup> shifts the hydroquinone oxidation by –285 mV (pH 8.8), and Ni<sup>2+</sup> by –194 mV (pH 9.16). The hydroquinone oxidation was shifted by –440 mV at pH 5 for Fe<sup>3+</sup> solutions examined up to pH 7. By contrast, reduction of the quinone is unperturbed by the presence of Cu<sup>2+</sup>, Ni<sup>2+</sup>, and Fe<sup>3+</sup> ions. Implications of these results to the mechanism of marine adhesion are discussed.

## Introduction

Marine organisms such as mussels, barnacles, limpets and kelp adhere to underwater surfaces through a complex series of chemical processes. An initial nonspecific adsorption via electrostatic, hydrogen bonding and van der Waals interactions, is followed by cross-linking of a secreted 3,4-dihydroxyphenylalanine (DOPA) containing peptide, Figure 1, and the substrate.<sup>1,2</sup> This then provides the well-known high adhesive strength common in marine biofouling organisms.<sup>1</sup> Cross-linking within the protein matrix, and between the matrix and the surface, is initiated by oxidation of *o*-diphenols (catechols) of DOPA to give a more reactive *o*-quinone center. The mechanisms of oxidation and cross-linking are not well understood, but they are thought to be initiated by enzymes such as catechol oxidase, with an undefined role being played by specific transition-metal ions.

What we do know is that the amount of Cu(II), Ni(II) and Fe(III), particularly in the byssus thread of mussels, is significantly greater in the DOPA protein matrix compared to ambient oceanic conditions.<sup>2</sup> Cupric ions are also known to act as a cross-linker between *o*-diphenols centers. This results in the expulsion of water from the adhesive matrix to increase the system rigidity in a similar, though less efficient, way to that caused by enzymatic formation of *o*-quinones.<sup>1</sup> The addition of ferric ions to an extract of mussel DOPA has been shown to coordinate three catechol centers that aerobically oxidize the protein, generating a reactive radical species that presents another possible method for attaching to a surface.<sup>2</sup> As such, an understanding of the electrochemistry of catechol (*o*-quinone)-containing proteins, coordinated to particular transition-metal ions, is central to our ability to define the chemistry of marine adhesion and this is the topic of this paper.

The electrochemistry of (uncoordinated) *p*-diphenol/quinone couples, and to a lesser extent the *o*-diphenol/quinone couples, is well studied in solution<sup>3</sup> and to a lesser extent on surfaces.<sup>4–6</sup> However, studies on a polymeric film containing DOPA residues immobilized on a carbon electrode have shown the catechol redox couple to be unstable during repetitive cycling between the fully oxidized and reduced forms.<sup>7,8</sup> A more recent study using a short chain alkanethiol self-assembled monolayer (SAM) containing terminal *o*-diphenol groups, without the amide linkage in the DOPA group, also suggests the instability of the catechol-quinone couple with repetitive potential cycling.<sup>9</sup> This instability is due to the quinone (or semiquinone) form of the couple, particularly at high pH, reacting further to produce undefined electroinactive products.

Cations are known to participate in bidentate coordination to *o*-diphenol by replacing the hydrogen atoms of the hydroxyl groups, O–M<sup>n+</sup>–O. By contrast, anion coordination with both monatomic and polyatomic anions results in a complex between the anion and the hydroxyl groups, OH–A<sup>m–</sup>–HO.<sup>10</sup> Both types of ion recognition events alter the optical properties of catechol, which then provides a basis for sensors for numerous types of ions. It is therefore not surprising that marine adhesive systems might also exploit ion-association events to achieve easier oxidation of DOPA groups in the protein matrix. Electrochemical studies have not been reported on the effect of Cu(II), Ni(II), and Fe(III) ion-association on the redox potential of surface-confined DOPA groups, although other model systems have noted that coordination of calcium, barium and magnesium to *o*-diphenol

(3) *Electrochemistry of Quinones*. By James Q. Chambers (Ch 12), in "The Chemistry of Quinonoid Compounds", Vol2 Patai, S. and Rappoport, Z. (eds). Wiley, 1988. NY.

(4) Trammell, S. A.; Lowry, D. A.; Seferos, D. S.; Moore, M.; Bazan, G. C.; Lebedev, N. *J. Electroanal. Chem.* **2007**, *606*, 33.

(5) Sato, Y.; Fujita, M.; Uosaki, K. *J. Chem. Soc., Faraday Trans.* **1996**, *92*, 3813.

(6) Ye, S.; Yashiro, A.; Sato, Y.; Uosaki, K. *J. Electroanal. Chem.* **2007**, *606*, 33.

(7) Tse, D. C. S.; Kuwana, T. *Anal. Chem.* **1978**, *50*, 1315.

(8) Ueda, C.; Tse, D. C. S.; Kuwana, T. *Anal. Chem.* **1982**, *54*, 850.

(9) Simmons, N. J.; Chin, K. O. A.; Harnisch, J. A.; Vaidya, B.; Trahanovsky, W. S.; Porter, M. D.; Angelici, R. J. *J. Electroanal. Chem.* **2000**, *482*, 178.

(10) Winstanley, K. J.; Sayer, A. M.; Smith, D. K. *Org. Biomol. Chem.* **2006**, *4*, 1760.

\* To whom correspondence should be addressed. Tel: 64-3-364 2100. Fax: 64-3-364 2110. E-mail: paula.brooksby@canterbury.ac.nz.

<sup>†</sup> Department of Chemistry, University of Canterbury.

<sup>‡</sup> Biological Sciences, University of Canterbury.

<sup>§</sup> The University of Adelaide.

(1) Fant, C.; Sott, K.; Elwing, H.; Höök, F. *Biofouling* **2000**, *16*, 119.

(2) Sever, M. J.; Weisser, J. T.; Monahan, J.; Srinivasan, S.; Wilker, J. J. *Angew. Chem., Int. Ed.* **2004**, *43*, 448.

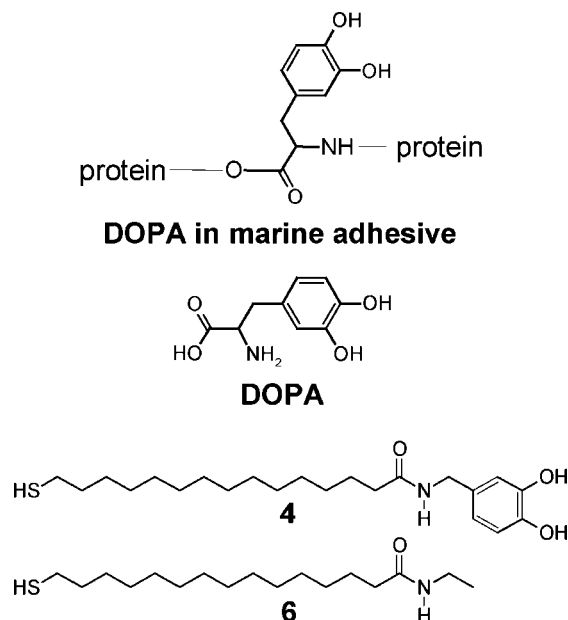


**Figure 1.** The chemical structures of the marine adhesive including the DOPA residue, DOPA, the electroactive hydroquinone for the model DOPA ( $\text{QH}_2$ ), **4**, and diluent, **6**.

enhances the electrocatalytic response for NADH oxidation.<sup>11</sup> These processes now require detailed analysis if we are to understand and exploit the adhesive properties associated with the oxidation of catechol.

In this study, a model for DOPA (Figure 1) was attached to the terminus of a long chain ( $\text{C}_{15}$ ) alkanethiol to give **4**. This was then assembled onto a polycrystalline gold surface as a SAM film to allow the study of ion-associated catechol electrochemistry. The diluent **6**, composed of the same alkanethiol without the catechol residue, was designed to isolate the model DOPA groups on the surface. A study of the electrochemistry of the (*o*-) hydroquinone/quinone couple, in pH 4–12, then provides important information on the redox properties and stability of the catechol group isolated at a surface.

Accumulation of Cu(II), Ni(II), and Fe(III) in the adhesive protein matrix of marine organisms, and its role in the electrochemistry of catechol groups, was investigated using the model DOPA interface. Cu(II), Ni(II) and Fe(III) association to surface catechols (model DOPA) was studied to elucidate the relationship between the identity of the cation and subsequent energy for the model DOPA oxidation reaction. This relationship was investigated over a wide pH range of 4–11, with the behavior between pH 8 and 9 being most relevant to oceanic conditions.

### Experimental Section

**Materials.** Dichloromethane was dried over  $\text{CaH}_2$  and freshly distilled under  $\text{N}_2$ , ethyl acetate was dried over  $\text{CaH}_2$  and freshly distilled under  $\text{N}_2$ , methanol (HPLC grade), ethanol (HPLC grade), *N,N*-dimethylformamide (DMF, <50 ppm water), diisopropyl ethylamine (DIPEA), *O*-(7-azabenzotriazol-1-yl)-*N,N,N'*-tetramethyluronium hexafluorophosphate (HATU), acetic acid, acetyl chloride, HCl,  $\text{HClO}_4$  (>70% AnalaR), 3,4-dimethoxybenzylamine, 16-Mercaptohexadecanoic acid, zinc dust, ethylamine hydrochloride,  $\text{MgSO}_4$ , NaCl,  $\text{NaClO}_4$ ,  $\text{NaHCO}_3$ ,  $\text{NH}_4\text{Cl}$ ,  $\text{BBr}_3$ , pet ether,  $\text{SiO}_2$ , and celite were purchased from Aldrich and used as received, unless otherwise stated. All buffer salts were purchased from Aldrich and used as received. Milli-Q water, conductivity >18  $\text{M}\Omega\cdot\text{cm}$ , was used for all aqueous solutions.

**Synthesis.** Syntheses of the model DOPA thiol and the diluent are given in the Supporting Information.

**Instrumentation.**  $^1\text{H}$  NMR spectra were recorded on a Varian Inova Spectrometer, operating at 500 MHz.  $^{13}\text{C}$  NMR spectra were recorded on a Varian Unity 300 spectrometer, operating at 75 MHz.

**Electrochemical Methods.** All electrochemical measurements were performed using an Eco Chimie Autolab PGSTAT302 (Netherlands) potentiostat. A standard glass three-electrode electrochemical cell that allows for continuous gas purging was used. A polycrystalline Au working electrode was fabricated and treated as described below. The working electrode was suspended in the electrochemical cell using the hanging meniscus method. This allows the front electrode surface to be in contact with the solution but without requiring the sides of the electrode to be insulated. A large area gold wire was used for the counter electrode, and an SCE was used for the reference electrode. Solutions were degassed with  $\text{N}_2$ , and all measurements were made at  $22 \pm 2$  °C. Voltammetric peak analysis was performed using the software package associated with the Autolab potentiostat.

**Gold Electrode Surface Preparation and Monolayer Formation.** Gold pieces (99.999% purity) were melted into a cylindrical ingot having a 6 mm diameter spherical planar surface. The surface was manually polished with successively finer grades of alumina on a microcloth, then thoroughly washed and sonicated in copious amounts of water. The front surface of the gold electrode was flame annealed using hydrogen gas to give a highly reflective interface. The electrode was cycled electrochemically in 0.01  $\text{M HClO}_4$  between the hydrogen and oxygen evolution regions ( $-0.25$  and  $1.45$  V (SCE) respectively) for 3 h and until successive cycles over a 10 min period did not give substantially changed voltammograms. The polycrystalline gold surface exhibited similar voltammograms to that of Au(210), and considered to be good quality. The surface roughness was determined to be 1.24 based on the amount of charge required to reduce a monolayer of gold oxide at a polycrystalline surface,  $400 \mu\text{C cm}^{-2}$ . Manual polishing was intermittently performed as required. Otherwise, the surface was cleaned between experiments by soaking the electrode in a piranha solution (*CAUTION: piranha solution is 1:3  $\text{H}_2\text{O}_2/\text{H}_2\text{SO}_4$  and is a strong oxidant of organic material*) for 20 min, followed by rinsing with water and flame annealing with hydrogen gas. The electrode was cooled and immediately immersed into an ethanolic thiol solution. The SAM films were prepared by dissolution of  $\sim 1$  mg/mL of the thiol(s) in ethanol, and immersing the gold electrode in this solution for not less than 2 days. The solutions contained either **4**, or a mixture of **4** with diluent **6** in a mole ratio of 20:1 (**6**:**4**). The chemical structures for DOPA and the electroactive thiol and diluent are given in Figure 1.

### Results and Discussion

The electrochemical properties and surface stability of the terminal catechol group were first examined by cycling the electrode potential between the fully oxidized and reduced forms [designated throughout as the quinone (**Q**) and hydroquinone ( $\text{QH}_2$ ), respectively] for pH 5 to 12. The redox signal from the catechol depends on which group,  $\text{QH}_2$  or **Q**, is present at the surface, which in turn depends on the pH of the solution. The redox response from a catechol group in the presence of Cu(II), Ni(II) and Fe(III) ions in the solution adjacent to the SAM was then investigated over a similar range of pH.

**Preliminary Considerations.** The stability of the entire alkanethiol SAM layer at Au is not the subject of this study. However, it is known that lengthening the alkyl linker between the thiol headgroup and the terminal redox center does increase the stability of the SAM due to attractive van der Waals interactions within the monolayer.<sup>12</sup> Thus a  $\text{C}_{15}$  alkyl linker was chosen for this study because it is long enough to provide sufficient interfacial stability to minimize possible disruptions to the SAM

(11) Raj, C. R.; Behera, S. *Langmuir* **2007**, *23*, 1600.

(12) Larsen, A. G.; Gothelf, K. V. *Langmuir* **2005**, *21*, 1015.

layer resulting from chemical and electrochemical reactions associated with the catechol group.

The length of an alkyl linker is known to influence the  $\text{QH}_2/\text{Q}$  redox peak separation ( $\Delta E_p$ );<sup>6,13</sup> at pH 1 a  $\text{C}_1$  linker for a *p*-hydroquinone group has a small separation of  $\sim 15$  mV, whereas the  $\text{C}_{12}$  linker has a peak separation of  $\sim 630$  mV.<sup>13</sup> Hence, the electron-transfer kinetics are reversible for short alkyl linkers and irreversible for longer linkers. Furthermore, the formal potential,  $E^\circ$ , (estimated as the average between the anodic and cathodic peaks) shifts by  $-16$  mV per  $\text{CH}_2$  unit. The negative  $E^\circ$  shift with increasing number of alkyl units indicates the cathodic peak center moves faster toward negative potentials than the anodic peak does toward positive potentials as the alkyl length increases.<sup>13</sup> This asymmetrical peak shift is attributed to the hydrophobicity of the redox centers. In particular, the quinone is more hydrophobic than the hydroquinone in acidic solutions, and is therefore more difficult to reduce compared to the oxidation of the hydroquinone.<sup>13</sup> Similar effects were expected with the *o*-hydroquinone terminated SAM used in this study. With these factors in mind we prepared SAMs containing **4** (with surface diluent **6**) and studied their electrochemistry in the presence of cations believed to have an important role in marine adhesive chemistry; Cu(II), Ni(II) and Fe(III).

The protonation state of catechol depends on solution pH. Speciation information for surface confined catechol is not known. However, solution speciation information is instructive as it provides a general notion for which quinone species may be present at any given pH. The speciation diagram for solution phase *o*-hydroquinone ( $\text{QH}_2/\text{QH}^-/\text{Q}^{2-}$ ) against solution pH is given in Supporting Information, Figure S2.<sup>14</sup> The proton speciation of solution DOPA shows the effect of ring substitution on hydroxyl protonation,<sup>15</sup> is to shift the  $\text{pK}_a$ 's by 1–2 pH units higher.

**Effect of pH on the Voltammetric Response of  $\text{QH}_2$ .** Figure 2A shows cyclic voltammograms for four mixed SAM (**4**: **6**) surfaces between pH 5 and 12, where each is normalized to its anodic peak current. A plot showing the values for  $E_{p,a}$ ,  $E_{p,c}$ , and  $E^\circ$  over a greater selection of pH conditions is shown in Figure 2B. The surface concentration ( $\Gamma_4$ ) varied between experiments due to slightly differing ratios of **4** to **6** in freshly prepared solutions, but was nevertheless in the range  $2.5\text{--}5.7 \times 10^{-11}$  mol  $\text{cm}^{-2}$ . The surface concentration of **4**, determined by integrating the area from the initial voltammogram assuming a 2-electron process, was compared to that of a similar compound  $\text{QH}_2(\text{CH}_2)_4\text{S-Au}$ :  $5.1 \times 10^{-10}$  mol  $\text{cm}^{-2}$ .<sup>13</sup> This suggests that the surface typically contains 5–11% coverage of the electroactive catechol groups, with the remainder being the diluent. Each catechol center, remote from its neighbors under these coverage conditions, is thus expected to behave, on average, as an isolated center.

Four distinct observations are evident from the results shown in Figure 2: (i) The plot of  $E^\circ$  against pH has a slope equal to 71 mV/pH, compared with a theoretical slope of 59 mV/pH for a 2-electron, 2-proton coupled process shown in equation 1: (ii)  $\Delta E_p$  is 376 mV at pH 12 and this increases to 1142 mV as the solution pH decreases to 5: (iii) The anodic peaks shifts with changing pH at a faster rate compared to the cathodic peak: (iv) The ratio of the anodic to cathodic peak heights becomes much greater than 1 as the pH increases. Point (iv) is addressed in a following section.

The solution  $\text{pK}_a$ 's for the catechol group in DOPA are 9.8 and 13.4.<sup>15</sup> Therefore, for  $\text{pH} < \sim 9$  the dominant catechol

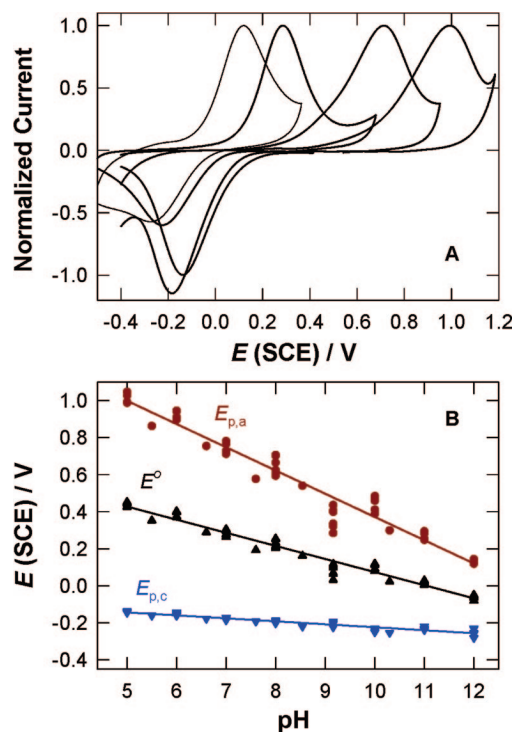
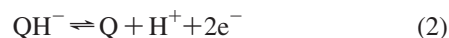
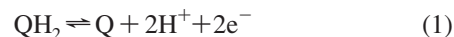


**Figure 2.** (A) Four voltammograms from a **4/6** mixed monolayer on Au at pH 5, 7, 9.16 and 12 (anodic peaks left to right respectively). Each voltammogram was normalized to its anodic peak current. Scan rate =  $50$   $\text{mV s}^{-1}$ . (B) The relationship between the redox peak centers, ( $\bullet$ )  $E_{p,a}$ , ( $\blacktriangledown$ )  $E_{p,c}$ , and the formal potential, ( $\blacktriangle$ )  $E^\circ$ , for pH solutions from 5 to 12. A linear regression analysis gave;  $E_{p,a} = -0.126\text{pH} + 1.626$  V;  $E_{p,c} = -0.016\text{pH} - 0.063$  V;  $E^\circ = -0.071\text{pH} + 0.782$  V.

derivative in the SAM will be  $\text{QH}_2$ . The oxidation of  $\text{QH}_2$  to  $\text{Q}$  is a 2-electron, 2-proton coupled process (eq 1).



The  $\text{QH}^-$  species should dominate the interface at  $\text{pH} > \sim 9$ , based on solution  $\text{pK}_a$  information, with its oxidation to  $\text{Q}$  being a 2-electron, 1-proton step (eq 2). At still higher pH,  $\text{Q}^{2-}$  will predominate at the surface, with a simple 2-electron oxidation giving  $\text{Q}$  (eq 3). In each of these pH intervals, bounded by the  $\text{pK}_a$ 's for the catechol species, the number of protons coupled to the oxidation step decreases, and there should be a corresponding change in the slope of the  $E^\circ$  - pH plot at the points that coincide with the surface  $\text{pK}_a$  for the quinoid derivative. Figure 2B shows that a slope change was not observed over the pH range examined. This indicates the  $\text{pK}_a$ 's of the surface catechol groups are much higher than their solution analogues. Moreover, it appears that the  $\text{QH}_2$  group is the dominant species for the isolated catechol group in the SAM up to pH 12. A similar result was found for surface catechols in which an amide linkage was not present.<sup>5,13</sup> The oxidation peak shown in Figure 2A has a small side peak observed at lower potential, which is intermittently present suggesting its occurrence is a function of surface conditions. This peak appears only in the pH range from 8 to 12. The significant scattering of data points in Figure 2B about pH 9–10 is attributed to observation, since the anodic peak potential was determined directly from the plot without further peak fitting. While the exact origins of the side peaks are unknown, their presence does indicate that some catechol groups are in a different surface environment to lower the catechol

(13) Hong, H. G.; Park, W. *Langmuir* **2001**, *17*, 2485.

(14) Powell, H. K. J.; Taylor, M. C. *Aust. J. Chem.* **1982**, *35*, 739.

(15) Pettit, L. *Pure Appl. Chem.* **1984**, *56*, 247.

oxidation energy. Catechol groups in close proximity to each other, possibly due to hydrogen bonding, would account for this observation. This is supported by the oxidation peak full width at half-height (fwhh) being  $\sim 300$  mV at pH 5 and 8, and  $\sim 310$  at pH 12. Also, in unbuffered solutions with low proton concentration, side peaks are observed and attributed to a change in the sequence of proton- and electron-transfer mechanism.<sup>5</sup>

The observed decrease in  $\Delta E_p$  with increased solution pH is thought to reflect the gradual change in the electron-transfer kinetics.<sup>13</sup> The solution environment is largely devoid of free protons under basic conditions, which assists with a simpler electron-transfer mechanism. The slope of the  $E_{p,c}$ -pH plot is only 16 mV/pH unit, thus the reduction of **Q** appears almost insensitive to the pH conditions. Conversely, the large slope from the anodic  $E_{p,a}$ -pH plot (126 mV/pH) indicates fewer protons than electrons are involved in the oxidation of **QH**<sub>2</sub>. However, the overall plot of  $E^{\circ}$ -pH is in keeping with a 2-proton 2-electron mechanism for the **QH**<sub>2</sub>/**Q** couple. The different slopes for  $E_{p,a}$ - and  $E_{p,c}$ -pH plots reflects the change in the electron-proton coupling reactions as described by Sato<sup>5</sup> and Trammell<sup>4</sup> for surface bound **QH**<sub>2</sub>/**Q** couple, with additional insight by Laviron<sup>16</sup> for the analysis of benzoquinone.

**Reactivity of the Q group and Stability of the Alkanethiol Layer.** Successful marine adhesion strategies involve the oxidation of the DOPA residue to a quinone, the reactive group that subsequently cross-links to other parts of the protein and to the surface. The reactivity of a quinone in the SAM can then be assessed by monitoring  $I_{p,c}$  (for the full and mixed SAMs), while repetitively cycling between the fully oxidized and reduced quinone. Hence, stability of the Au-S bond in the monolayer is necessary if the reactivity of the **Q**, and stability of the **QH**<sub>2</sub>/**Q** couple, is to be examined.

A continual loss of the quinone signal has been observed with repeat cycling for a short chain (C<sub>4</sub>) SAMs containing a terminal **QH**<sub>2</sub> group, and this has been partly attributed to displacement of the thiol by complex anion buffer salts, and increased solubility of deprotonated hydroquinone and oxidation products.<sup>13</sup> This is probably true for short chain thiols, but the longer alkanethiol used in this study is expected to provide much greater film stability. The resulting monolayers were allowed to assemble for not less than two days, and the quality of the layers was examined by electrochemical impedance spectroscopy (EIS) and voltammetry of the Ru(NH<sub>3</sub>)<sub>6</sub><sup>3+/4+</sup> redox probe in solution.

Typical impedance and voltammetric results for a full monolayer of **4**, before and after cycling the electrode between the fully oxidized and reduced quinone forms for 15 min at pH 5, are shown in Figure 3. The electron-transfer response of the ruthenium redox probe across the SAM **4** was typical of a fully blocking monolayer that remains almost unchanged after cycling the electrode between the **QH**<sub>2</sub>/**Q** redox couples. However, the voltammogram of a redox probe at a defective monolayer may appear normal at low scan rates. Nyquist plots provide more robust evidence that a monolayer is present on the surface. The absence of a Warburg impedance in the studied frequency range indicates that the monolayer forms a good barrier on the surface to prevent the direct approach of ruthenium to the surface. The radius of the semicircle decreases after potential cycling, which suggests a reduced charge transfer resistance across the film. Structural changes at the film interface are to be expected when the terminal groups of the SAM react (laterally) with nearby groups (vide infra), resulting in interfacial disordering. This might explain the reduced charge transfer resistance through the film. The Bode plot,  $\log Z' - \log f$ , shows changes are more pronounced

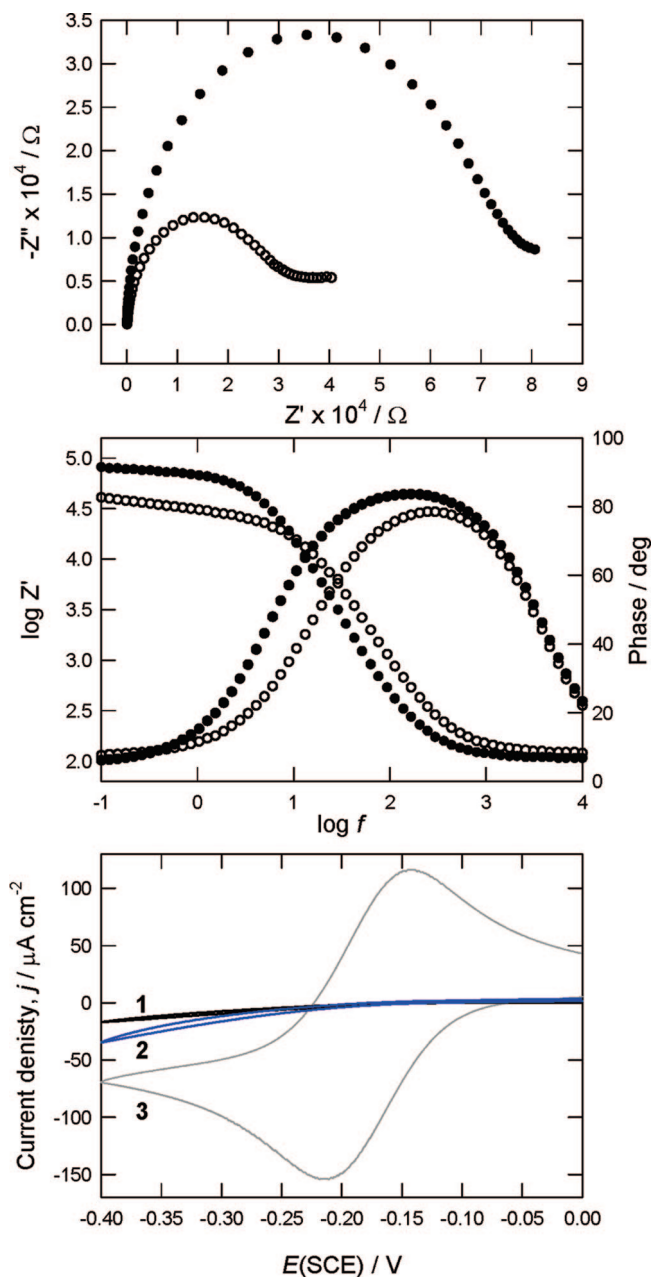


**Figure 3.** (top) Complex plane impedance plot and (middle) a Bode plot recorded at  $-0.18$  V for a full monolayer of **4** in 1 mM Ru(NH<sub>3</sub>)(ClO<sub>4</sub>) + 0.2 M acetate/acetic acid buffer, pH 5, before (solid symbols) and after (open symbols) oxidation of the monolayer at 0.8 V for 15 min. (bottom) Cyclic voltammograms of a full monolayer of **4** in 1 mM Ru(NH<sub>3</sub>)(ClO<sub>4</sub>) + 0.2 M acetate/acetic acid buffer, pH 5, solution before (1) and after (2) oxidation of the monolayer at 0.8 V for 15 min, and at the bare Au electrode (3). Scan rate = 50 mV s<sup>-1</sup>.

in the low frequency region, where mass transport is the rate controlling step. Thus, changes to the charge transfer resistance reflect potential induced changes to the film structure, and there is no evidence for significant thiol desorption from the Au surface.

Deactivation of the quinone was monitored by measuring the **Q** reduction peak current,  $I_{p,c}$ , with repetitive cycling between oxidation and reduction potentials. Figure 4 shows typical trends observed for  $I_{p,c}$ , normalized to the initial cycle,  $I_{p,c}/I_{p,c(0)}$ . The peak potential and fwhh was unchanged for repeat cycles during the reduction. In general, similar current trends are observed for the  $I_{p,a}/I_{p,a(0)}$  peaks (not shown), but the anodic peak potential shifts to more positive values, and fwhh increases, with repeat cycles. Nonetheless, the total area of the anodic peak decreases

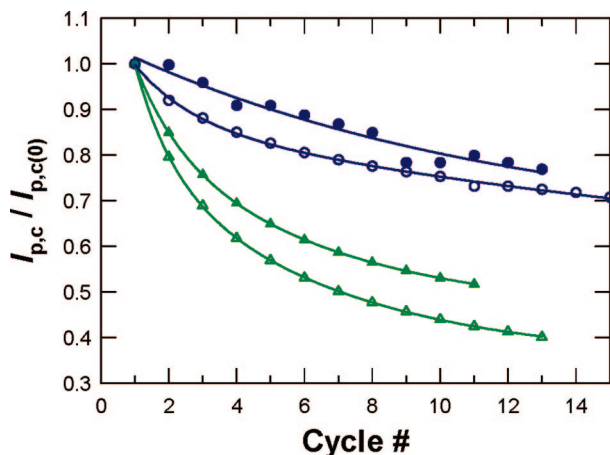


**Figure 4.** Plot of the cathodic peak current normalized to the height from the first cycle,  $I_{p,c}/I_{p,c(0)}$ , against the number of voltammetric cycles for full ( $\blacktriangle, \triangle$ ) and mixed ( $\bullet, \circ$ ) monolayers of **4**. The solution pH was 5 (closed symbols) or 9.16 (open symbols). Data taken from voltammograms run at  $50 \text{ mV s}^{-1}$ .

with repeat cycles. The rate of signal loss is significantly greater with a full monolayer, and incrementally faster at higher pH. At pH 14, and with a full monolayer, normalized peak currents were below 0.3 after only 4 cycles. Similar rapid deactivation was observed with quinones on polymer-supported carbon surfaces.<sup>8</sup> In solution, charged quinoid species are known to react with the parent hydroquinone to form new molecules that are often electrochemically inactive.<sup>3,8</sup> Thus, at the surface, a full monolayer of **4** has (hydro)quinone neighbors that likely participate in similar chemical deactivation pathways. Mixed monolayers have (hydro)quinone centers isolated within a plane of methyl groups and these clearly participate in the deactivation of the quinone, but by an indeterminate route. The increased longevity of radical and anionic quinoid species in alkaline solutions provides increased probability for surface deactivation. This is also evident in the peak current ratios,  $I_{p,a}/I_{p,c}$  for alkaline solutions always being greater than 1 compared to the ratio in acidic solutions, Figure 2A. Thus it appears that loss of the redox peaks for the  $\text{QH}_2/\text{Q}$  with continual potential cycling between the fully oxidized and reduced forms, Figure 4, is due to the irreversible reaction of the terminal quinoid groups to electroinactive products, and not from thiol desorption off the surface.

Thus, oxidation of  $\text{QH}_2$  to a reactive  $\text{Q}$ , provides one route to cross-linking within the model DOPA. The rate of reaction is dependent on the identity of the neighbor, with a (hydro)quinone group reacting faster than a methyl, and the solution pH. The role of particular metal ions in the catechol oxidation mechanism was thus examined.

**Metal-Ion Association at the  $\text{QH}_2$  Surface with pH Modulation.** The influence of low concentrations of metal ions Cu(II), Ni(II) and Fe(III) on the redox behavior of mixed SAMs was investigated, since accumulation of these ions, and the concurrent oxidation of DOPA peptides in the secretions of marine adhesives are well documented, see introduction. In particular, Cu(II) ions, in the presence of oxygen, are known to catalyze the oxidation of *o*-hydroquinone to quinone and hydrogen peroxide.<sup>17</sup> The likely complication from uncontrolled oxygen content to the redox response for  $\text{QH}_2$  was removed in this study by ensuring that all solutions were purged free of oxygen prior to electrochemistry. However, it should be noted that oxygen is abundantly present in oceanic conditions. Speciation diagrams

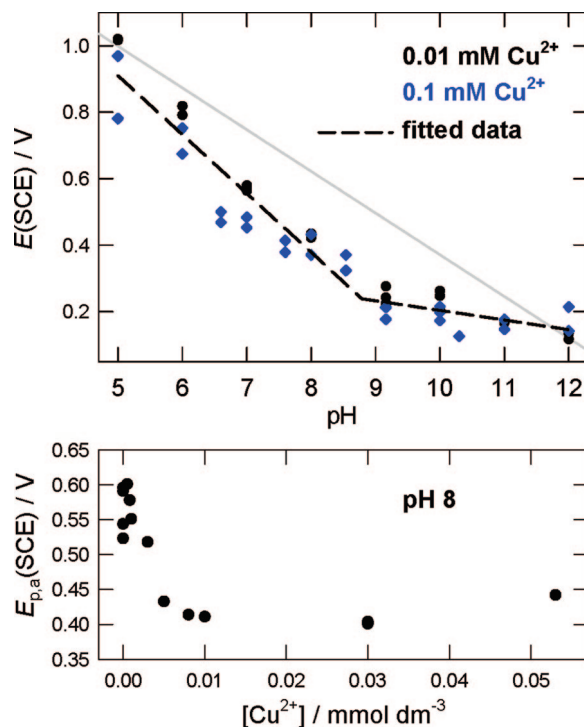


**Figure 5.** (top) A plot showing the relationship between the anodic peak center,  $E_{p,a}$ , for pH solutions from 5 to 12 containing 0.01 mM (black circles) and 0.1 mM (blue circles)  $\text{Cu}(\text{NO}_3)_2$ . The data were fitted to 2 piecewise linear functions (dotted line) giving  $E_{p,a}$  (pH  $\leq 9$ ) =  $-0.177\text{pH} + 1.796 \text{ V}$  and  $E_{p,a}$  (pH  $> 9$ ) =  $-0.029\text{pH} + 0.494 \text{ V}$ . (bottom) A plot showing the relationship between  $E_{p,a}$  and  $0 \text{ mM} \leq [\text{Cu}^{2+}] \leq 0.053 \text{ mM}$  at pH 8. Data taken from voltammograms run at  $50 \text{ mV s}^{-1}$ .

for the hydroxides of Cu(II), Ni(II) and Fe(III), and solution Cu(II)–DOPA, Ni(II)–DOPA systems are given in the Supporting Information, Figures S3 and S4, respectively. Iron is not soluble in solution when the pH is greater than  $\sim 3$  and as such iron was complexed with EDTA to keep it soluble. Solution Fe–EDTA–DOPA speciation diagrams are also provided in Supporting Information. The speciation diagrams were constructed using  $1 \mu\text{mol dm}^{-3}$  concentrations for all reactants except for Ni–DOPA, where the DOPA concentration was  $100 \mu\text{mol dm}^{-3}$ , and the constants given in Table S1.

In solution,  $\text{Cu}^{2+}$ ,  $\text{Ni}^{2+}$  and  $\text{Fe}^{3+}$  association to DOPA occurs at  $6 < \text{pH} < 12$ ,  $8 < \text{pH} < 11$ , and  $\text{pH} < 7$  (with EDTA), respectively. Otherwise, free metal ions in acidic solution, or metal-hydroxide species in basic solutions, predominate. The number of catechol ligands about the central metal species in solution can vary from 1 to 3 depending on the relative ratio of metal ion to ligand. Isolated  $\text{QH}_2$  centers of the mixed SAM interface are expected (but not confirmed) to give a 1:1 ratio of metal ion: catechol in the relevant pH range, with the remaining metal ligand position(s) taken up by hydroxide(s) and water (or EDTA).

Plots showing the values for  $E_{p,a}$  for 0.01 and 0.1  $\text{mmol dm}^{-3}$  solutions of  $\text{Cu}^{2+}$  for  $5 \leq \text{pH} \leq 12$  and the relationship between  $E_{p,a}$  and  $0 \text{ mM} \leq [\text{Cu}^{2+}] \leq 0.053 \text{ mM}$  at pH 8 are shown in Figure 5, top and bottom, respectively. The  $\text{QH}_2$  oxidation peak is sensitive to  $[\text{Cu}^{2+}]$  as low as  $5 \mu\text{mol dm}^{-3}$ , hence the copper ion concentrations used in this study were well above the lower detection limit depicted in Figure 5(bottom). Figure 6 depicts plots of  $E_p$ –pH that show values for  $E_{p,a}$ ,  $E_{p,c}$ , and  $E^0$  for 0.1  $\text{mmol dm}^{-3}$  solutions of  $\text{Ni}^{2+}$  for  $5 \leq \text{pH} \leq 12$ , and  $\text{Fe}(\text{EDTA})^{3+}$  for  $\text{pH} < 7$ . The gray trend lines in Figures 5 (top) and 6 represent overlaid fitted results from Figure 2B.

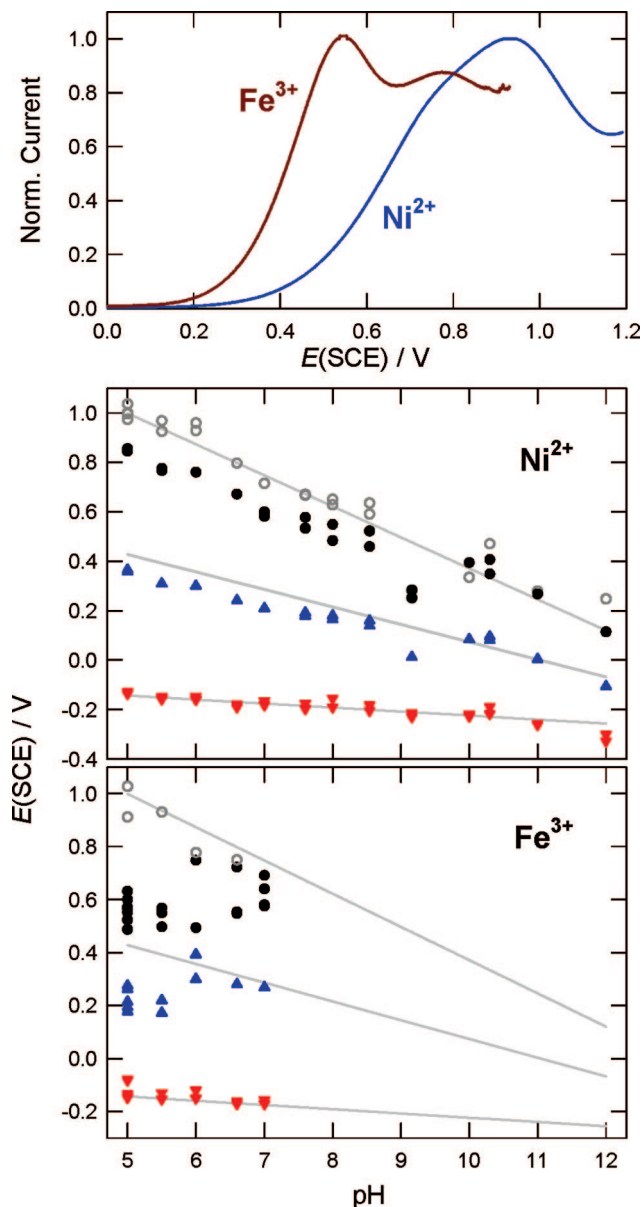


**Figure 6.** (top) Two curves showing typical anodic peaks observed during cyclic voltammetry of mixed monolayers of **4** in the presence of  $\text{Ni}^{2+}$  (pH 6) and  $\text{Fe}^{3+}$  (pH 6.6) salts. Scan rate =  $50 \text{ mV s}^{-1}$ . (middle) A plot showing the relationship between (●)  $E_{p,a1}$ , (○)  $E_{p,a2}$ , (▼)  $E_{p,c}$ , and (▲)  $E^0$  for pH solutions from 5 to 12 containing  $0.1 \text{ mM Ni}(\text{NO}_3)_2$ . Peak 1 represents metal-quinone associated centers and peak 2 the unassociated quinone centers. (bottom) A plot showing the relationship between (●)  $E_{p,a1}$ , (○)  $E_{p,a2}$ , (▼)  $E_{p,c}$ , and (▲)  $E^0$  for pH solutions from 5 to 12 containing  $0.1 \text{ mM Fe}(\text{NO}_3)_3$ . Peak 1 represents metal-quinone associated centers and peak 2 the unassociated quinone centers. Data taken from voltammograms run at  $50 \text{ mV s}^{-1}$ .

Expressions for  $\Delta E^0$  ( $=\Delta E^0_{\text{complex}} - \Delta E^0_{\text{ligand}}$ ) for redox active ligands complexed to a metal ion have been described.<sup>18</sup> These equations (not given) describe solution phase species that are dependent on the metal ion concentration, the metal to ligand ratio, the coordination of ligand following electron-transfer, and the stability constants of the metal-ligand complexes. The oxidation potential of the coordinated catechol, for a solution phase study of  $\text{Al}^{3+}$  coordinated to catechol, occurs at more positive potential compared to uncoordinated catechol.<sup>19</sup> The observed positive  $\Delta E^0$  was attributed to the  $\text{Al}^{3+}$  stabilization

of the ligand toward oxidation due to electrostatic interactions between the catecholate and the hard metal center. However,  $\Delta E^0$  was insensitive to the  $\text{Al}^{3+}$  concentration, which is not in keeping with predictions based on the above-mentioned equations.<sup>19</sup> Thus, the failure of the predictive qualities in solution, suggests that such expressions must be regarded as unsuitable for surface events.

**Copper Association to  $\text{QH}_2$ .** The data in Figure 5 (top) were fitted to two piecewise linear functions (see dotted lines) to give a slope for  $E_{p,a}$  ( $\text{pH} \leq 9$ ) =  $-177 \text{ mV/pH}$  and  $E_{p,a}$  ( $\text{pH} > 9$ ) =  $-29 \text{ mV/pH}$ . These simplistic linear fits are sufficient to model the data to a first approximation, although the acid-base behavior is certainly more complicated. At low pH, copper underpotential deposition occurs at electrode potentials near that for **Q** reduction. Each scan was initiated at sufficiently positive potential to avoid copper electrodeposition, but this meant reduction of **Q** was not possible in solutions containing  $\text{Cu}^{2+}$  ions. Reduction of **Q** was accomplished by removing the electrode to a new solution at the same pH, but without copper. The **Q** was then reduced at  $-0.4 \text{ V}$  for 10 s, the electrode returned to a  $\text{Cu}^{2+}$  solution, and voltammetry continued. In sufficiently alkaline solutions,  $\text{pH} > 9.16$ , copper electrodeposition occurs at a potential more negative than the reduction of **Q**. Thus with  $\text{pH} > 9.16$ , **Q** reduction is measurable in solution containing free  $\text{Cu}^{2+}$  ions, and  $E_{p,c}$  was unchanged from those measured in the absence of  $\text{Cu}^{2+}$  (not shown).

The presence of copper in solution has two effects on the associated electrochemistry of **4**: First, it lowers the  $\text{QH}_2$  oxidation potential, where the  $E_{p,a}$  shifts by 60 mV at pH 5, and by 285 mV at pH 8.8, which correspond to a lowering of the Gibbs's free energy from  $-12$  to  $-55 \text{ kJ}$ , respectively. The slope of the pH dependent  $\text{QH}_2$  oxidation potential is  $177 \text{ mV/pH}$ , a value greater than that observed in the absence of copper over the same pH region ( $126 \text{ mV/pH}$ ). Second, a change to the slope of the fitted data is observed at pH 8.8. This change in slope from  $177$  to  $29 \text{ mV/pH}$  is significant. The slope of the  $E^0$  ( $\text{pH} > 8.8$ ) with pH was determined to be  $24 \text{ mV/pH}$  based on the measured **Q** reduction potential in this region.

Speciation information for Cu complexes with DOPA (Figure S3, Supporting Information) indicates that  $\text{Cu}(\text{DOPA})$  coordination does not occur when the pH is less than 6. However,  $E_{p,a}$  values for  $\text{pH} < 6$  (Figure 5(top)) show copper ions are interacting with the surface catechol. Measured  $E_{p,a}$  values are expected to be unperturbed in the absence of any ion-association. Ion-association events are well-known to occur between metal cations and electronegative centers of small organic species.<sup>20</sup> The strength of ion association interactions largely depends on the charge-to-radius ratio of the ion, the electron density of the second association site of the couple, and whether or not multiple association centers are involved. Surface bound catechol is protonated at low pH such that ion association can occur as depicted by the three scenarios in Figure 7 (left). The hydroxylation of the metal center depends on the solution pH.

Results for the  $0.1 \text{ mmol dm}^{-3} \text{ Cu}^{2+}$  data set (Figure 5) hint at an inflection point about pH 6–7, which is likely due to a change in the ion-association environment of free  $\text{Cu}^{2+}$  to  $\text{Cu}(\text{OH})^+$ . This is in keeping with either the addition of a proton to the metal center (as an OH group), or a decrease to the charge-to-radius ratio for the cation (by OH ligand addition). The inflection point is speculative at this time, with the overall  $\text{QH}_2$  oxidation behavior in Figure 5(top) being well described by simple

(18) Shiu, K. K.; Harrison, D. J. *J. Electroanal. Chem.* **1989**, *260*, 249.

(19) Downard, A. J.; O'Sullivan, B.; Powell, K. J. *Polyhedron* **1996**, *15*, 3469.

(20) Ronald Fawcett. W. "Liquids, Solutions and Interfaces: From Classical Macroscopic Descriptions to Modern Microscopic Details" Oxford University Press (US), 2004.

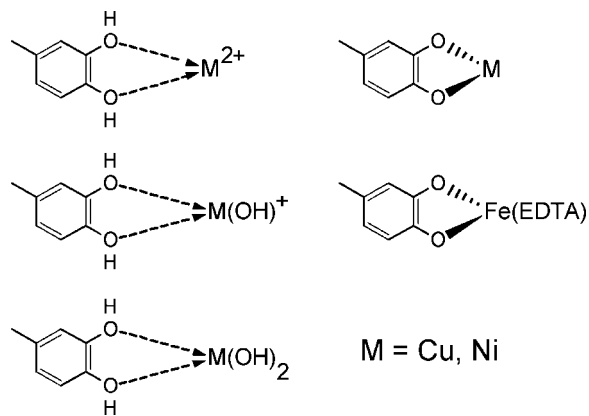


**Figure 7.** Schematic representation of metal ion-association to  $\text{QH}_2$  compared to metal coordination and deprotonation of the catechol.

$\text{Cu}^{2+}$  ion association. The resulting Cu-quinone complex is shown schematically in Figure 7 (top right). Loss of hydroquinone protons from this species, with subsequent coordination to the  $\text{Cu}^{2+}$ , results in redox peaks that are insensitive to pH changes,  $\text{pH} > 8.8$ . The persistence of a small slope (29 mV/pH) can have several origins, including the presence of uncoordinated  $\text{QH}_2$  or ion-associated  $\text{Cu}(\text{OH})_2$  centers.  $\text{Cu}(\text{OH})_2$ , which is the dominant species at high pH, is not expected to strongly associate with surface  $\text{Q}^{2-}$  groups. Measurements at  $\text{pH} > 12$  are required to ascertain if  $\text{Cu}(\text{OH})_2$  continues to influence the surface  $\text{Q}^{2-}$  electrochemistry in the pH region.

Copper had no observable effect on  $\text{Q}$  reduction at  $9.16 < \text{pH} < 12$ , neither was there a change in the relative ratio for  $I_{\text{p,a}}/I_{\text{p,c}}$  (not shown). Both observations suggest that cations are either not associated with the  $\text{Q}$  oxygens, or if associated, do not affect the reduction energy. Minimal association between the  $\text{Cu}(\text{OH})_2$  and oxygen centers is likely based on electrostatic considerations.

These results clearly indicate that  $\text{Cu}^{2+}$  association to isolated  $\text{QH}_2$  centers decreases the energy required for oxidation by comparison to unassociated  $\text{QH}_2$ . This then facilitates oxidation to a reactive  $\text{Q}$  center. An optimal pH for this interaction of 8.8, (based on the fitted data) corresponds to the largest  $E_{\text{p,a}}$  shift (285 mV) and a Gibbs' free energy change ( $\Delta G$ ) =  $-55$  kJ. This pH is close to typical oceanic pH conditions. Thus, in the marine environment, enzyme-initiated oxidation of  $\text{Cu}(\text{DOPA})$  residues is a plausible mechanism that allows adhesion to commence.

**Nickel Association to  $\text{QH}_2$ .** The voltammetric results obtained for  $\text{Ni}^{2+}$  and  $\text{Fe}(\text{EDTA})$  (see below) consistently display 2 oxidation peaks,  $E_{\text{p,a1}}$  and  $E_{\text{p,a2}}$ , Figure 6(top). Peak splitting,  $E_{\text{p,a2}} - E_{\text{p,a1}}$ , for  $\text{Ni}^{2+}$  associated  $\text{QH}_2$  was moderate at 160 mV at pH 5. The two oxidation peaks are almost coincident for  $\text{pH} > 9$  and as such the determination of the peak centers required curve fitting. Peak  $E_{\text{p,a2}}$  traces the line observed for  $\text{QH}_2$  oxidation from Figure 2B. Hence, the origin of peak  $E_{\text{p,a2}}$ , is attributed to the oxidation of the hydroquinone centers not associated with  $\text{Ni}^{2+}$ . The fact that Ni does not electrodeposit onto the surface under the conditions used here, allows  $E_{\text{p,c}}$  to be measured, and hence,  $E^{0'}$  to be calculated. The gray trend lines plotted with  $E_{\text{p,c}}$  and  $E^{0'}$ -pH data are those previously shown in Figure 2B.

Trend lines were not fitted to the Ni data because it could be fitted with either a single linear slope or 2 piecewise linear functions similar to that observed for the copper system, and neither can be fully justified at this time because the  $E$ -pH slope change at pH 9 is not significant. Furthermore, at pH 9, there is a consistently only a single observed oxidation peak that is attributed to  $E_{\text{p,a1}}$ . The largest potential shift, between the metal associated and unassociated  $\text{QH}_2$  groups is 194 mV ( $\Delta G = -37$

kJ) and occurs at a pH ( $\sim 9$ ) predicted to give the greatest amount of  $\text{Ni}(\text{DOPA})$  in solution see Figure S4. As for the copper system, charged species are present (Ni and Ni-hydroxide in this case) when the pH is less than  $\sim 9$ . These then associates with the  $\text{QH}_2$  (Figure 7) to reduce the energy required for  $\text{QH}_2$  oxidation. Neutral  $\text{Ni}(\text{OH})_2$  dominates the solution composition for pH greater than  $\sim 9$  resulting in minimal interaction at the C-OH and C=O centers.

The magnitude of the oxidation peak shifts show  $\text{Ni}^{2+}$  is not as effective as  $\text{Cu}^{2+}$  in decreasing the oxidation potential for  $\text{QH}_2$ . The existence of two catechol oxidation peaks in the  $\text{Ni}^{2+}$  SAM system indicates that two types of surface  $\text{QH}_2$  groups are present. One has  $\text{QH}_2$  associated to  $\text{Ni}^{2+}$  while the other remains unassociated. The optimal conditions for favorable association (coordination) between  $\text{Ni}^{2+}$  and surface  $\text{QH}_2$  occur for pH 9–10, where this pH gives the largest peak shift for  $E_{\text{p,a1}}$ , and an absence of  $E_{\text{p,a2}}$ . In addition,  $\text{Ni}^{2+}$  ions have no measurable effect on  $\text{Q}$  reduction electrochemistry.

**Iron Association to  $\text{QH}_2$ .** The speciation calculations shown in Figure S4 confirm (as expected) that the stability of aqueous  $\text{Fe}^{3+}$  solutions containing EDTA is poor when the  $\text{pH} > 7$ . Noticeable changes to the solution color occur within the time frame of solution degassing (30 min), which is indicative of  $\text{Fe}(\text{OH})_{3,s}$  formation. Therefore, voltammetry was restricted to solutions with the  $\text{pH} \leq 7$ . This pH range is not beneficial to marine systems, but nature has developed many ways to sequester ferric ion from the environment, which is then stabilized via a host of mechanisms for later release. The coordination of  $\text{Fe}^{3+}$  to surface  $\text{QH}_2$  groups was investigated within the pH limitations described above, that is, below pH 7 and in  $\text{Fe}(\text{EDTA})$  solutions.

The voltammetric results for **4** are similar to those obtained for the Ni system with the appearance of two  $\text{QH}_2$  oxidation peaks in the presence of  $\text{Fe}(\text{EDTA})$ , with  $E_{\text{p,a1}}$  and  $E_{\text{p,a2}}$  assigned to the coordinated and uncoordinated Fe-(hydro)quinone centers (Figure 7). The reproducibility of peak  $E_{\text{p,a1}}$  was poor between pH 6 and 7, with the peak center migrating as much as 250 mV between repeat trials. The origin of this variability is unknown, but it is speculated to be due to solution decomposition, and possibly contamination of the SAM interface with Fe particulates. The slope of the  $E_{\text{p,a1}}$ -pH plot is indeterminate given the poor stability of  $E_{\text{p,a1}}$ . However, the value for  $E_{\text{p,a1}}$ , at the two lowest pH points, 5 and 5.5, are consistently near 0.550 mV, indicative of  $\text{QH}_2$  deprotonation following Fe coordination. Fe coordinated  $\text{QH}_2$  gave the largest peak shift of 440 mV ( $\Delta G = -85$  kJ) at pH 5 compared to Cu, 285 mV ( $\Delta G = -55$  kJ) at pH 8.8, or Ni, 194 mV ( $\Delta G = -37$  kJ) at pH 9.16.

The Fe(III) species clearly had the greatest effect on the oxidation potential and the reduction potential for  $\text{Q}$  was unaltered by the ferric solution. Ferric ion is coordinated to EDTA as the neutral molecule when the  $\text{pH} < 7$  and this complex is unlikely to associate with the C=O centers.

The single oxidation peak for copper solutions, and doublets for nickel and iron, suggests the hydroquinone sites are occupied with copper ions and only partially occupied in the nickel and iron ion systems. However, thus far no account of the lability of the metal ions has been included. Copper is expected to be more labile on the surface, based on water exchange rates for each metal.<sup>21</sup> Thus, even if some fraction of the surface  $\text{QH}_2$  sites are not occupied with copper, only one oxidation peak would be observed simply because the copper-ligand association-dissociation kinetics is fast on the time scale of the electrochemical experiment. The much less labile, and more inert, nickel and iron metals<sup>21</sup> would be expected to occupy only some fraction of

(21) Casey, W. H.; Swaddle, T. W. *Rev. Geophys.* **2003**, *41*, 40.

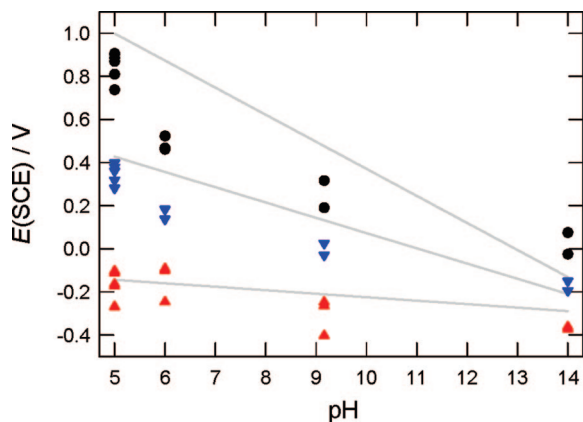


**Figure 8.** Relationship between the redox peak centers, (●)  $E_{p,a}$ , (▼)  $E_{p,c}$ , and the formal potential, (▲)  $E^o$ , for selected pH solutions from 5 to 14 for a full monolayer of **4**. The gray trend lines are taken from Figure 4B. Data taken from voltammograms run at 50 mV s<sup>-1</sup>.

surface  $\text{QH}_2$  sites, but the slower metal–ligand association–dissociation kinetics from these ions allow observation of both occupied and unoccupied  $\text{QH}_2$  groups. At this time, it is unknown whether this kinetic effect determines the origin of the single or double oxidation peaks, or whether each metal–ligand species has differing concentration profiles at the interface.

**Surface Coverage and Redox Potential of  $\text{QH}_2$ .** The voltammetric response from the electrochemistry for monolayers of **4** without diluent was examined under selected pH conditions and the results are shown in Figure 8, with the gray trend lines representing the fitted data in Figure 2B. From these results it is apparent that both the oxidation,  $E_{p,a}$ , and reduction,  $E_{p,c}$  peaks shift to more negative potentials. Moreover, the  $E_{p,a}$  shift with pH is not parallel to the isolated  $\text{QH}_2$  centers. Rather, the trend is similar to the electrochemical response displayed with the metal-associated hydroquinone centers. Lowering the oxidation energy barrier, and hence increasing the reduction energy barrier, is likely related to the increased hydrophilicity at the interface. An exchange of terminal methyl groups of a diluent for hydroxyl groups of the catechol changes the dielectric properties of the interface. It is well-known that dielectric properties of an interface affect both kinetic and thermodynamic reactions confined to this region, and thus it is not surprising that the oxidation and reduction potentials are similarly influenced.<sup>22</sup>

## Conclusions

The actual protein matrix of the marine adhesive varies according to the different species.<sup>23</sup> The arrangement and number of repeat units of amino acids are thought to play different roles, such as providing regions of hydrophilicity or charge density variation to assist with matrix organization or initial adsorption events. An initial physisorption step is followed by an adhesion process involving oxidation of catechol to the quinone. This facilitates covalent bonding to a substrate with associated cross-linking of protein strands within the adhesion matrix. Oxidation is brought about by specific enzymes and possibly molecular oxygen. Cross-linking (curing) within the matrix changes the mechanical properties of the glue. The cross-linking agents include

polyvalent transition metal ions, oxygen, aldehyde and many polyfunctional cross-linkers.<sup>23,24</sup> Transition metal ions have at least three significant roles in marine systems. (i) Catechol groups (in the DOPA moiety) coordinate to the metal ions, thus lowering the oxidation energy. (ii) Polyvalent metal ions provide a mechanism for cross-linking. (iii) The metal can facilitate adsorption of protein to a surface by acting as a metal center about which DOPA and substrata are coordinated (ligands).

The environment about the  $\text{QH}_2/\text{Q}$  couple in the 2-dimensional planar surface of the SAM interface is appreciably different from the 3-dimensional network of the DOPA environment in marine adhesive secretions. The model DOPA surface coordinates one metal to one catechol center, assuming each catechol is spatially isolated in the SAM. However, the marine adhesive matrix can cross-link up to three catechol ligands for each metal ion. Nonetheless, the redox properties of the  $\text{QH}_2/\text{Q}$  couple have been shown to be significantly affected by the properties of the electrical double layer, the chemical identity of the nearest neighbors, and the presence of  $\text{Cu}^{2+}$ ,  $\text{Ni}^{2+}$ , and  $\text{Fe}^{3+}$  ions. The oxidation energy of catechol at the model DOPA interface, constructed using **4** and diluent with **6**, was shown to decrease upon association with  $\text{Cu}^{2+}$ ,  $\text{Ni}^{2+}$ , and  $\text{Fe}^{3+}$  ions. The decrease was measured by a shift in the oxidation potential of the catechol to negative values. The magnitude of the potential shift depends on the solution pH and the identity of the cation. At oceanic relevant pH conditions,  $\text{Cu}^{2+}$  gave the greatest change in energy, followed by  $\text{Ni}^{2+}$ , with  $\text{Fe}^{3+}$  not determined at pH > 7. By contrast, the reduction of the quinone was insensitive to  $\text{Ni}^{2+}$  and  $\text{Fe}^{3+}$ , and to  $\text{Cu}^{2+}$  when the pH > 9. These results provide valuable insight into the electrochemistry of DOPA oxidation and marine adhesion that until now have not been examined in detail.

The stability of **Q** depends on the nature of the SAM interface and the solution pH. The deactivation of **Q** is rapid at high pH and when the SAM surface contains other hydroquinone functionalities. This provides evidence for a high degree of lateral cross-linking in the SAM, with similar reactions expected to occur in the natural protein matrix.

Future efforts to reveal the electrochemical properties of marine adhesive proteins will benefit from model chemical structures that are more closely related to the protein matrix. The evolving chemical processes generated by species interacting with settlement surfaces are often considered to be a “black box” of processes that are important but little-understood. Understanding these adhesion processes is fundamental to clarifying how marine organisms are capable of attaching quickly, and remaining attached, in often-turbulent, wave-driven conditions.

**Acknowledgment.** We thank the Royal Society of New Zealand Marsden fund, Contract No. UOC306, for their generous support.

**Supporting Information Available:** Synthesis and characterization of the model DOPA and diluent thiols, the speciation diagram for  $\text{QH}_2/\text{QH}^-/\text{Q}^{2-}$  in aqueous solutions between 4 < pH < 14, speciation diagrams for the hydroxides of  $\text{Cu}^{2+}$ ,  $\text{Ni}^{2+}$ ,  $\text{Fe}^{3+}$ , and  $\text{Fe}(\text{EDTA})$  complexes with, and without, DOPA between 2 < pH < 12, and the table of constants used to derive the speciation figures. This material is available free of charge via the Internet at <http://pubs.acs.org>.

LA8007816

(22) Kwon, Y.; Mrksich, M. *J. Am. Chem. Soc.* **2004**, *124*, 812.

(23) Silverman, H. G.; Roberto, F. F. *Mar. Biotechnol.* **2007**, *9*, 661.

(24) Deming, T. J. *Current Opin. Chem. Biol.* **1999**, *3*, 100.